Geophysical Research Letters

RESEARCH LETTER
10.1029/2018GL079794

Crustal Deformation and Seismicity Modulated by Groundwater Recharge of Karst Aquifers

N. D'Agostino[1], F. Silverii[2], O. Amoroso[3], V. Convertito[4], F. Fiorillo[5], G. Ventafridda[6], and A. Zollo[7]

[1]Istituto Nazionale Geofisica e Vulcanologia, Rome, Italy, [2]Scripps Institution of Oceanography, University of California, San Diego, La Jolla, CA, USA, [3]Department of Physics E.R. Caianiello, University of Salerno, Fisciano, Italy, [4]Istituto Nazionale Geofisica e Vulcanologia, Naples, Italy, [5]Dipartimento di Scienze e Tecnologie, University of Sannio, Benevento, Italy, [6]Approvvigionamento Idrico (DIRAP), Acquedotto Pugliese S.p.A., Bari, Italy, [7]Department of Physics E. Pancini, University of Naples Federico II, Naples, Italy

Key Points:
- Phases of recharge/discharge of karst aquifers modulate strain and seismicity in the Southern Apennines (Italy)
- We invert GPS time series to model hydrological stress perturbations by karst aquifers
- The 1980 Irpinia, M_S 6.9, earthquake occurred during favorable hydrological stress conditions

Supporting Information:
- Supporting Information S1
- Data Set S1
- Movie S1

Correspondence to:
N. D'Agostino,
nicola.dagostino@ingv.it

Citation:
D'Agostino, N., Silverii, F., Amoroso, O., Convertito, V., Fiorillo, F., Ventafridda, G., & Zollo, A. (2018). Crustal deformation and seismicity modulated by groundwater recharge of karst aquifers. *Geophysical Research Letters*, *45*, 12,253–12,262. https://doi.org/10.1029/2018GL079794

Received 27 JUL 2018
Accepted 8 NOV 2018
Accepted article online 14 NOV 2018
Published online 26 NOV 2018

Abstract Triggered seismicity in karst regions has been explained assuming the existence of a hydraulically connected fracture system and downward diffusion of surface pore pressures. Karst systems are, in fact, able to swiftly channel large amount of rainfall through networks of conduits increasing the hydraulic head loading upon the fluid-saturated, poroelastic crust. Here we use Global Positioning System and hydrological and seismicity data to show that poroelastic strain in the shallow crust (0–3.5 km) controls seasonal and multiannual modulation of seismicity along the Irpinia Fault Zone (Southern Italy) without requiring a hydraulically connected fracture system from the surface to hypocentral depths. We suggest that groundwater recharge of karst aquifers along the Irpinia Fault Zone produces stress perturbations large enough to modulate strain accumulation and seismicity and temporarily modify the probability of nucleation of seismic events such as the 1980 Irpinia, M_S 6.9, earthquake.

Plain Language Summary Redistribution of water masses on the surface of the Earth has long been known to alter the state of stress in the crust and trigger seismicity. Karst aquifers form in chemically soluble bedrock, mostly carbonate rocks. In these aquifers most of the rain and snowmelt water infiltrates underground and contributes to climatically modulated groundwater recharge. In this study we use Global Positioning System measurements, together with accurate location of earthquakes, to show that crustal deformation and seismicity in the tectonically active Southern Apennines (Italy) are modulated by seasonal and multiannual phases of groundwater recharge of karst aquifers. The small stress variations induced by hydrological forcing add to the long-term tectonic loading and help to illuminate the behavior of the Irpinia Fault Zone which, on 23 November 1980, produced the largest Italian event in the last 100 years (magnitude 6.9).

1. Introduction

Variations of the spatial and temporal distribution of hydrological masses deform the lithosphere (van Dam et al., 2001) and modulate stress buildup in active fault zones (Ader et al., 2014). One of the most obvious manifestations of hydrological forcing is expressed by modulations of seismicity (Heki, 2003; Saar & Manga, 2003) triggered by stress variations as small as a few kilopascals (Christiansen et al., 2007). Two mechanisms have been proposed to explain triggering of seismicity in response to hydrological forcing. The first predicts instantaneous elastic stress perturbation at depth as a consequence of hydrological loading (Bettinelli et al., 2008; Heki, 2003). The second mechanism requires the existence of a hydraulically connected fracture system. Pore pressure variations, altering the strength of the faults, reach hypocentral depths after a time lag dependent on the hydraulic diffusivity (Roeloffs, 1988; Saar & Manga, 2003). Due to the capacity of channeling large amount of water in the conduits network, karst aquifers rapidly develop large increases in hydraulic head after rainfall. This property has been invoked to explain rainfall-triggered seismicity (Miller, 2008). A statistically significant causal relationship has been proposed based on fluid diffusion and rate-and-state-dependent frictional nucleation (Hainzl et al., 2006). However, it is unclear if seismicity is only due to pore pressure diffusion or may also be triggered in response to poroelastic solid stress changes (Segall, 1989) which may overcome the shortcomings associated with the requirement of a hydraulically connected fracture system to

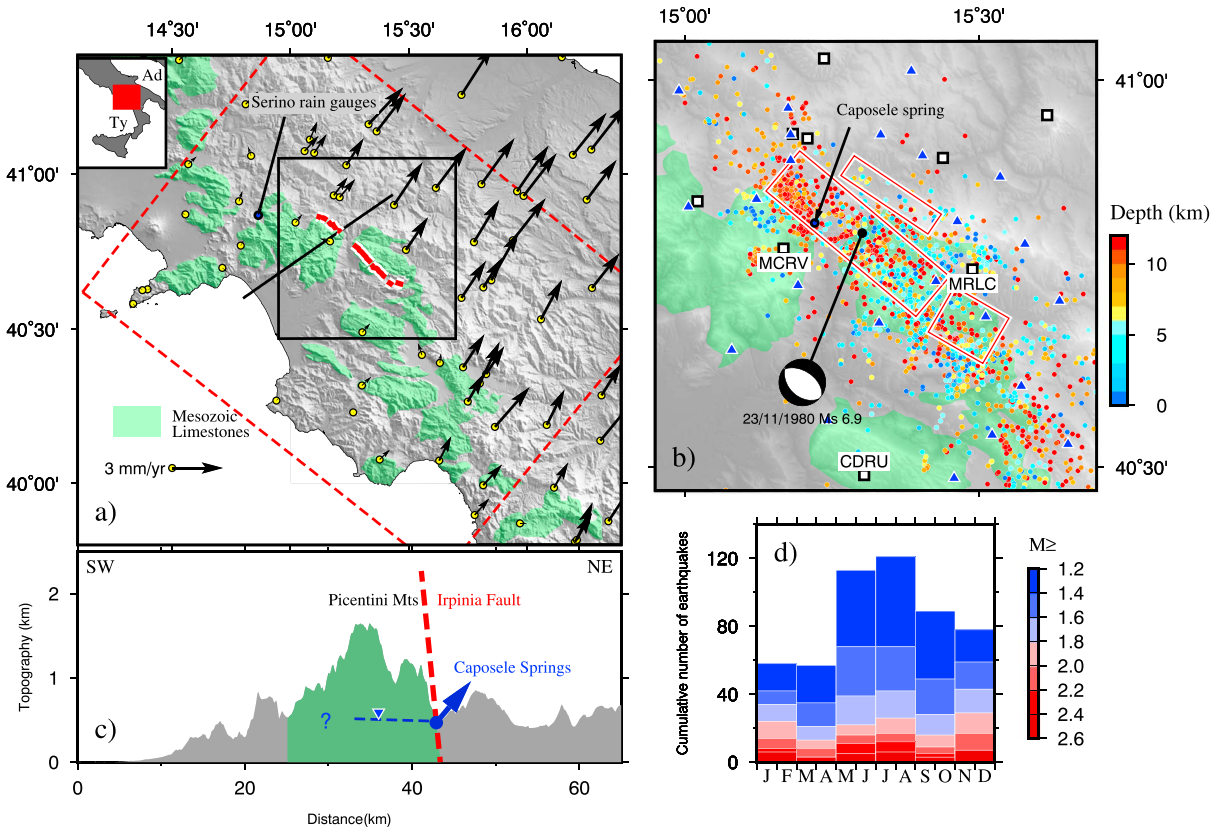

Figure 1. (a) Shaded topography and Global Positioning System velocities in a Tyrrhenian reference frame (D'Agostino, 2014). The red dashed line encloses the area used for strain modeling. The trace of Irpinia Fault Zone from Galli and Peronace (2014) is shown in red. Carbonate rocks are emphasized in green. (b) Inset map (area enclosed by the black line in a) showing 2008–2017 seismicity from the Irpinia Seismic Network (stations represented as blue triangles). Global Centroid Moment Tensor project focal solution and surface projections of the three segments activated during the 23 November 1980, M_S 6.9, event. (c) Topographic profile (trace shown as a black line in a) and simplified hydrogeological scheme of the Caposele spring. The blue dashed line and the reversed triangle show the hypothetical elevation of the water table within the karst aquifer. (d) Two-month binned histogram of the 2008–2017 seismicity.

seismogenetic depths. An important aspect concerns the extent to which this process is relevant for the nucleation of large earthquakes. Along the Mediterranean-Alpine belt, large parts of tectonically active countries (Italy, Balkans, and Turkey) are underlain by carbonate rocks where hydrological forcing from groundwater recharge in karst aquifers provides the opportunity to discriminate alternative models and investigate the modulation of stress buildup and seismicity. Here we comprehensively investigate the mechanism relating groundwater storage, stress buildup, and seismicity in the Southern Apennines (Italy) exploiting the concurrent presence of karst regions with dense seismic and geodetic networks. It is within this context that we finally assess the hydrological contribution to the 1980 Irpinia, M_S 6.9, earthquake.

2. Geological and Hydrogeological Framework

Historical seismicity, Quaternary faulting and geodetically measured ~3 mm/year SW-NE extension show that active deformation in the Southern Apennines (Figure 1a) defines a coherent, northwest-southeast alignment of activity (D'Agostino, 2014; Galli & Peronace, 2014; Rovida et al., 2016). The 23 November 1980 Irpinia, M_S 6.9, earthquake was a complex, normal faulting event rupturing three distinct fault segments (Bernard & Zollo, 1989) comprehensively called IFZ (Irpinia Fault Zone, Figure 1a). The event ruptured through a stack of rootless nappes overthrusted over the Mesozoic carbonates of the Apulia Platform (AP) (Nicolai & Gambini, 2007). Active and passive seismological investigations and boreholes suggest that fluid-saturated, clay-rich mélange zone at the top of AP (depth 3.5–4 km in the IFZ area) defines an efficient barrier to fluid circulation between the oil-producing AP carbonates at depth and the overlying, extensively fractured allochthonous units (Amoroso et al., 2014). The Caposele spring (417 m a.s.l; Figures 1b and 1c) has a mean annual discharge of about 4 m^3/s, drains directly the saturated zone of an aquifer composed of fractured Mesozoic limestones, and is bounded, to the northeast, by the IFZ. As no man-made modifications occur in its catchment, this spring

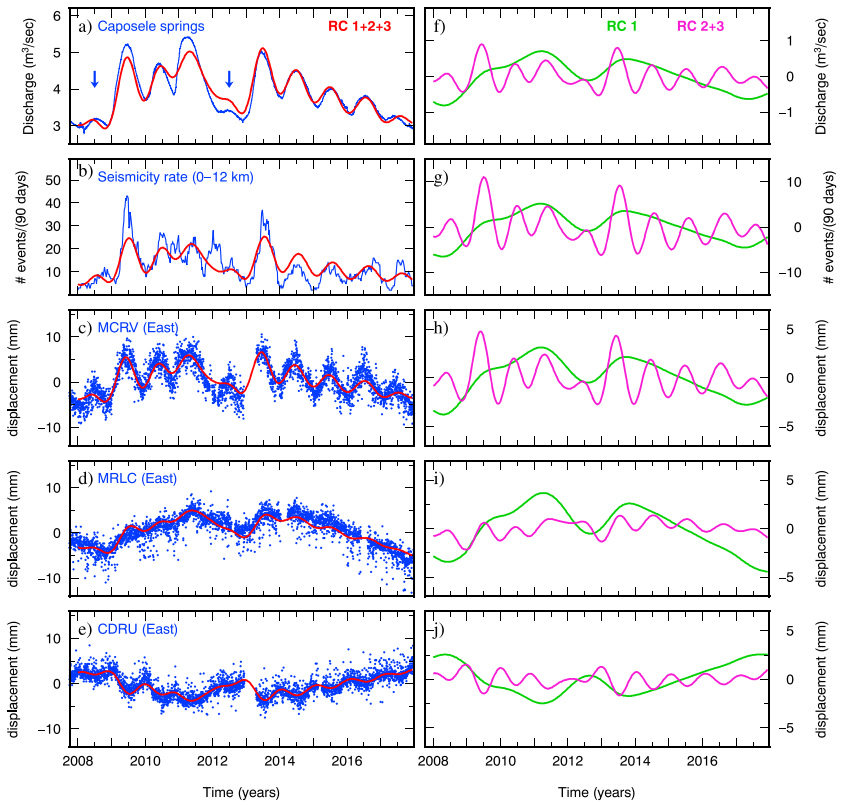

Figure 2. (a) Spring discharge of the Caposele spring (in blue, location in Figure 1). Arrows indicate drought years. (b) Declustered seismicity rate (in blue, calculated in 90-day sliding windows. (c–e) East component detrended Global Positioning System displacements from sites MCRV, MRLC, and CDRU (blue circles; locations in Figure 1b). Red lines in (a–e) show the summation of the first three reconstructed components (RC) as determined by Multichannel Singular Spectrum Analysis. (f–j) Show separately the first three reconstructed components. RC2 and RC3 form an oscillatory seasonal signal and are shown together. RC1 is a long-term multiannual signal common to all the five time series.

is strictly controlled by climate trends (Allocca et al., 2014). The peaks of maximum discharge (Figure 2a), corresponding with high hydraulic head in the aquifer, occur in spring-summer (May–July), some (4 to 5) months after the period of maximum precipitation, whereas the minimum discharge takes place during the rainy months (November–December). Drought years (2008 and 2012) are typically characterized by reduced discharge during the entire hydrological year (Figure 2a). The smooth shape of the hydrograph and its delayed response to rainfall indicate that spring discharge is not affected by single events of rainfall (Fiorillo, 2009). Here we argue that these characteristics, shared by the largest karst aquifers in the Apennines (Fiorillo et al., 2015), allow the buildup of significant hydraulic head modulating stress accumulation and seismicity rates on the IFZ.

3. Seismicity and GPS Data

The 2008–2017 seismicity (Figure 1b and supporting information for details) along the IFZ is characterized by low-magnitude events ($-0.1 \leq M_L \leq 3.9$), mostly concentrated at depths smaller than 15 km (supporting information Figure S2), dispersed within a crustal volume including the fault segments activated during the 1980 M_S 6.9 earthquake (De Matteis et al., 2012). To avoid biases related to seasonal variations of network sensitivity and aftershock clustering, we select events above the magnitude of completeness (*Mc* 1.2) and decluster the catalog. A more detailed discussion of the applied methodologies can be found in the supporting information (Aki, 1965; Amoroso et al., 2014; Lomax et al., 2000, 2009; Reasenberg, 1985; Schorlemmer & Gerstenberger, 2007; Shi & Bolt, 1982; Wiemer, 2001; Woessner & Wiemer, 2005). After these steps the seismicity is preferentially concentrated (61%) in the May–October semester (Figure 1d). A 90-day sliding average consistently displays seasonal peaks of seismicity in July–August and two prominent peaks in 2009 and 2013 corresponding to substantial groundwater recharge following drought years (Figure 2b). Separation of seismicity

in two different depth ranges shows that peaks of seismicity at 0–6 km are essentially in phase with spring discharge whereas delayed 0.1–0.2 years at 6–12 km (supporting information Figure S3).

Time series of crustal displacements from permanent Global Positioning System (GPS) stations show the occurrence of seasonal and multiannual modulation of extensional strain transients near to karst aquifers with a distinct temporal correlation with phases of groundwater recharge (Silverii et al., 2016). A description of GPS data and analysis can be found in the supporting information (Avallone et al., 2010; Bertiger et al., 2010; Blewitt et al., 2016; Métois et al., 2015; Rebischung et al., 2012). Peak-to-peak seasonal variations (maximum in May–June) exceed 5–10 mm of northeastward displacement for GPS sites located northeast (Figures 2c and 2d) of the largest karst aquifers. The sites located to the southwest (Figure 2e) show an opposite behavior, resulting in maximum horizontal seasonal dilatation in late spring/early summer centered on karst aquifers. A complementary study shows that this behavior is found throughout the Apennines where limestone lithologies allow the development of karst aquifers (Silverii et al., 2019).

We use Multichannel Singular Spectrum Analysis (Ghil et al., 2002) to investigate forcing patterns shared by spring discharge, seismicity, and GPS displacements time series (see supporting information for details). Multichannel Singular Spectrum Analysis can be considered as an extension of classical Principal Component Analysis and exploiting the spatial and temporal correlation of geophysical signals; it extracts transient deformation, seasonal oscillations, and background noise from multivariate time series without a priori knowledge about their period and amplitude or their spatiotemporal structures. We use spring discharge, seismicity rate, and GPS data, in the time interval 2008–2018 covered by all data time series (Figure 2), selecting the three GPS stations (location in Figure 1a) on the basis of data continuity and intensity of the seasonal/multiannual signals. Figures 2f and 2j show the three most significant components from the five data series. The combined reconstructed components RC2 and RC3 represent a seasonal oscillation, whereas RC1 represents a longer, multiannual signal with a poorly constrained 4- to 5-year time scale. The amplitude-modulated seasonal oscillation consistently displays the largest amplitudes in the same years (2009 and 2013) for the different observables. It therefore appears that both annual and multiannual hydrological signals are present and reveal a strong correlation in time with surface displacements and seismicity rates.

4. Seismicity, Strain, and Hydrological Forcing

The hypothesis of seismicity modulation associated to the elastic response of the lithosphere to hydrologic loading conflicts with Gravity Recovery and Climate Experiment observations indicating maximum total hydrological loading in December–January, 5–6 months earlier than the increase in seismicity rate (Silverii et al., 2016). The positive correlation between horizontal strain transients with phases of maximum groundwater recharge appears, instead, more consistent with a poroelastic process. We assess the role of pore pressure diffusion with simple models of crustal diffusivity. In case of harmonic variations of the hydrological forcing, diffusivity c can be estimated from the time lag between peaks of surface pressure and seismicity rate at depth z using the relation (Saar & Manga, 2003):

$$c = \frac{Tz^2}{4\pi t^2} \tag{1}$$

where t is the observed time lag and T is the forcing period (1 year for seasonal variations). A time lag of 0.1–0.2 years between spring discharges, used as a proxy for hydraulic head at the surface, and seismicity at depth of 6–12 km (supporting information Figure S3) yields diffusivities in excess of ~10 m^2/s, a value generally considered as the upper range of observed crustal diffusivity (Talwani et al., 2007). Suprahydrostatic pressures in the AP at depths > 4 km estimated from boreholes logging and seismological analyses (Amoroso et al., 2017; Improta et al., 2014), however, conflict with the idea of a high-permeability fracture system hydraulically connected from the surface to the deepest hypocenters (~12-km depth).

This evidence prompts us to posit the existence of a layered hydromechanical structure in which a high-permeability upper layer (<3.5 km) at hydrostatic pore pressures overlies a lower layer where suprahydrostatic pore pressures are maintained by the low-permeability barrier at the top of AP. The high permeability causes the upper layer to expand horizontally almost instantaneously in response to the increase of hydraulic head in karst aquifers. The underlying elastic crust is driven into horizontal extension by elastic coupling

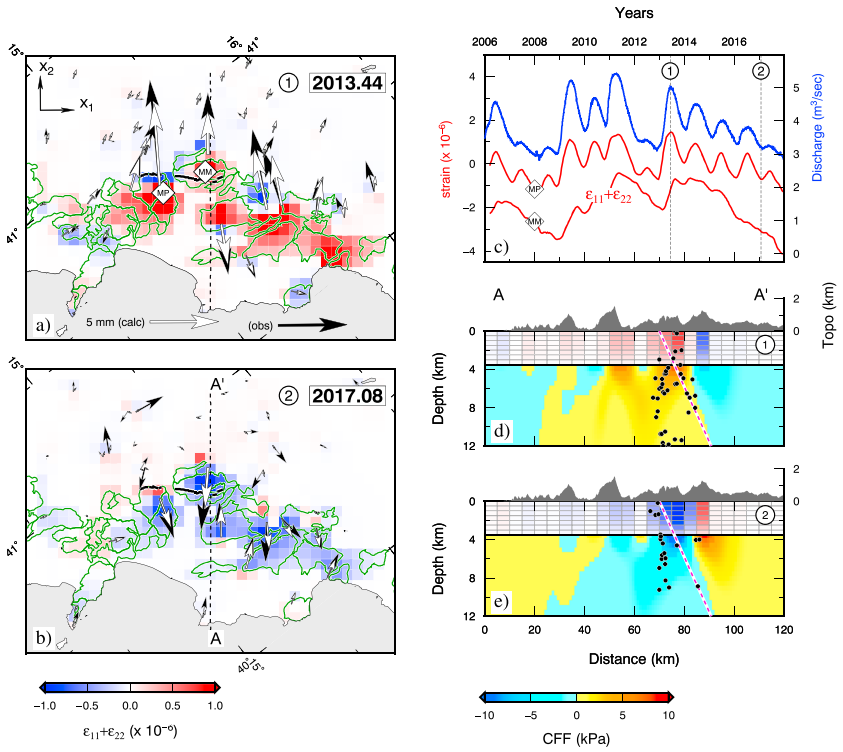

Figure 3. (a, b) Maps of distributed hydrological strain with calculated/observed Global Positioning System displacements. The complete, continuous strain evolution is shown in supporting information Movie S1. The two frames display opposite conditions of groundwater recharge in karst aquifers (green lines) and opposite dilatational patterns. (c) Time series of calculated strain (red lines) in two distinct locations (MM, Monte Marzano and MP, Monti Picentini) compared with Caposele spring discharge (blue, locations in Figure 1). (d, e) Cross sections (trace in a and b) across the Irpinia Fault Zone (dashed red line) showing dilatational strain in the upper layer (0–3.5 km) and the Coulomb failure function stress perturbations (evaluated on a N310, 60° dipping normal fault) in the underlying elastic half-space.

(Segall, 1989), allowing stress perturbations to occur instantaneously without the need of direct pore pressure diffusion. We test the hypothesis of hydrological-driven stress using Green's function approach employing analytical solutions for the displacement, strain, and stress of elementary cuboid sources (Barbot et al., 2017). The method of Barbot et al. (2017) separates out the anelastic component of strain from the elastic strain to calculate the effect of anelastic deformation (including poroelastic effects) within an elastic body allowing us to calculate the stresses, displacements, and strains produced by pore fluid pressure variations within an elastic matrix. We invert detrended GPS time series to estimate the temporal evolution of the ϵ_{11} and ϵ_{22} strain tensor components in a three-dimensional grid of cuboid sources extending to a depth of 3.5 km and calculate the stress perturbations induced in the underlying elastic half-space. To impose smoothness constraints and avoid unreasonable distributions of strain, we applied a Laplacian operator in the vertical and horizontal directions and an additional operator to penalize strain on cuboid sources not directly overlain by karst areas (see supporting information for details on the modeling). Our observations and inversion approach have poor depth resolution, and strain monotonically decreases with depth down to the limit of cuboid sources, consistent with the hypothesis of hydraulic head loading upon a fluid-saturated, poroelastic crust (Figure S6). Figures 3a and 3b show two frames extracted from the 2006–2018 strain time series (continuous time series are shown in Movie S1). These two episodes are representative of episodes of maximum and minimum dilatational strains corresponding to a high/low groundwater recharge conditions, respectively. The good agreement between observed and calculated displacements and the opposite sign of deformation in response to high/low phases of groundwater recharge yield a plausible spatial and temporal connection between hydrological forcing of karst aquifers and the observed deformation. The comparison between Figures 1a and 3 shows that alternating contractional and extensional NE-SW hydrological strain transients temporally modulate the similarly oriented NE-SW extensional tectonic strain accumulation along the IFZ.

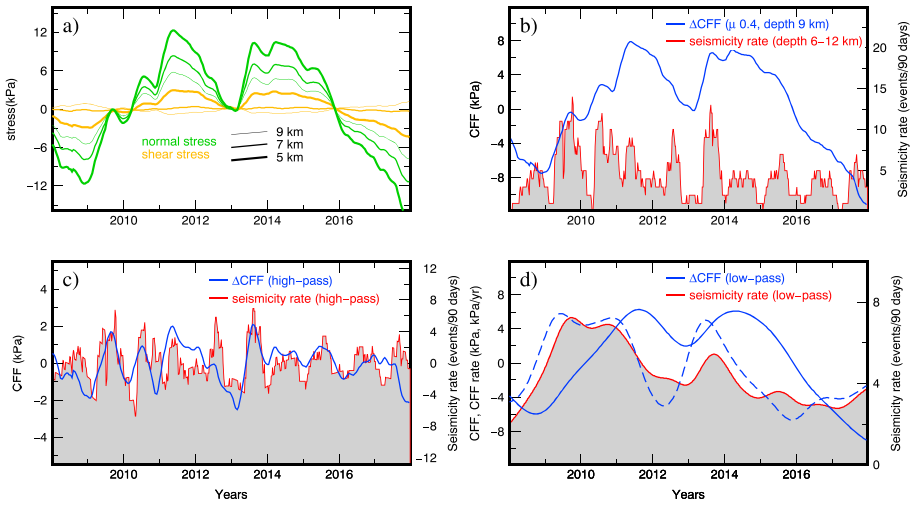

Figure 4. (a) The 2008–2018 hydrological stress perturbations resolved as shear and normal stresses on a N310, 60° dipping normal fault at various depths (5, 7, and 9 km). (b) CFF stress (blue line) calculated using $\mu = 0.4$ at a depth of 9 km compared to seismicity rate at 6- to 12-km depth. (c) Same as (b) but after application of high-pass filtering (Gaussian 6σ width = 2.5 years). Seasonal seismicity peaks correlate with CFF. (d) Same as (b) but after application of low-pass filtering. Multiannual seismicity peaks correlate with time derivative of CFF rates (dashed line). CFF = Coulomb failure function.

5. Seismicity Response to Hydrological Stress Perturbations

We calculate stress perturbations as shear and normal stresses (tensile stresses positive) on a N310, 60° dipping normal fault in consideration of the prevalent focal solutions of large (Figure 1) and small (De Matteis et al., 2012) earthquakes and express these as variations in the Coulomb failure function (CFF) given a friction coefficient $\mu = 0.4$ (see supporting information for details). Results show that peak-to-peak seasonal and multiannual CFF stress perturbations of 5–10 kPa occur beneath the karst aquifers down to 10-km depth (Figures 3d and 3e). We evaluate the seismicity response to stress perturbation (Figure 4) in the southwestern part of the IFZ (cross sections in Figure 3) where events are relatively equally distributed between the top of AP and 12-km depth. Perturbations of calculated CFF stresses as large as 4–5 and 10–15 kPa for seasonal and multiannual time scales, respectively, extend to depth of ~10 km (Figures 4b and 4c) and are mainly contributed by variations of normal stress (Figure 4a). If the stress forcing function is given by a hydrological harmonic component of magnitude b and period T superimposed on a linear term a, periodic reversal and decreasing stress accumulation occur if $a < 2\pi b/T$ (Ader et al., 2014). Geodetic estimates (D'Agostino, 2014) of secular NE-SW extensional strain rate on IFZ equal $40–60 \times 10^{-9}$ year^{-1} resulting in CFF secular stress loading rate of 2–4 kPa/year (see supporting information) on the IFZ. These values imply that $a < 2\pi/T$ at both seasonal and multiannual time scales. Stress accumulation is thus significantly accelerated, relative to the secular rate, during seasonal and multiannual phases of groundwater recharge, and the opposite occurs during phases of groundwater discharge supporting the hypothesis of seasonal and multiannual seismicity modulation.

The response of seismicity to harmonic stress perturbations is evaluated in the framework of the rate and state friction theory (Ader et al., 2014). Rate and state and finite fault models exhibit two regimes in their seismicity response to periodic stress perturbations. Both the amplitude (β) and phase (ϕ) of the change in seismicity rates depend on the relationship between the period of the stress perturbation (T) and a critical period (T_a). Seismicity correlates with stress perturbations ($\phi \approx 0$) at periods $T < T_a$whereas it correlates with the rate of stress perturbations ($\phi \approx \pi/2$) for $T > T_a$ with the characteristic period separating the two regimes being $T_a = 2\pi t_a$, where t_a is the rate and state nucleation time. The amplitude β of the seismic response is maximum at $T \approx T_a$ and decreases with both smaller and larger periods as $T \to 0$ and $T \to \infty$, respectively. Stress variations along the southwestern part of the IFZ are dominated by the multiannual signal (Figure 4b). The phase of the seismicity response, however, appears to change with the period of the stress perturbation. By separating high (seasonal, $T = 1$ year) and low (multiannual, $T = 4–5$ years) frequency stress perturbations, we observe different responses of the seismicity. Seasonal seismicity (Figure 4c) correlates with stress perturbations ($\phi \approx 0$), whereas low-pass multiannual variations of seismicity (Figure 4d) correlate with periods of stress increase ($\phi \approx \pi/2$). This observation shows that the response of seismicity changes with the period of

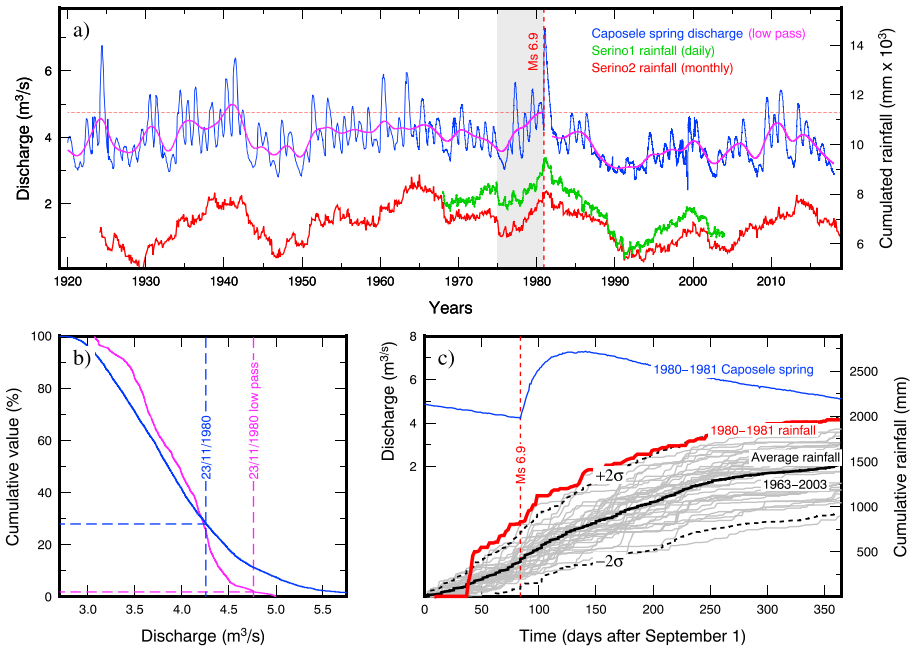

Figure 5. (a) The 1920–2018 Caposele spring discharge data (blue line) and its low-pass value (pink, Gaussian 6σ width = 5 years) filtered to suppress the effect of seasonal oscillations. Daily and monthly rainfall data from two distinct rain gauges at Serino (location in Figure 1a) shown as cumulative sums over the preceding 5 years. Both discharge and rainfall data indicate an increasing recharge conditions in the 5 years (gray area) before 23 November 1980. (b) Reverse cumulative distribution of the 1920–2018 spring discharge values. The raw value observed on 23 November 1980 is exceeded by 28.0% of the observations, whereas its low-pass, filtered value is exceeded only by 1.1% of the observations. (c) The 1963–2003 cumulative daily rainfall time series (gray lines) from Serino rain gauge for individual hydrological years (1 September to 31 October) and their average (black, dashed $\pm 2\sigma$). Exceptional rainfall (red line) released one third (~500 mm) of the average yearly cumulative rainfall between 9 and 13 October 1980. The discharge at Caposele spring only increased after the earthquake.

stress perturbation consistently with $1 < T_a < 4–5$ years. Figure 2g indicates that the amplitude of seismicity response (β) is slightly more sensitive to seasonal than multiannual oscillations indicating that T_a is probably closer to 1 year. This situation appears to be intermediate between rapidly deforming regions as Nepal (Bettinelli et al., 2008), where $T_a \approx 1$ year, and intraplate areas, such as the New Madrid Seismic Zone (Craig et al., 2017), where $T_a \geq 10$ years. In light of significant uncertainties and approximations of simple models of elastic stress and earthquake nucleation, we emphasize that the proposed scenario provides only a first-order, plausible interpretation connecting hydrological forcing, stress perturbations, and seismicity.

6. Hydrological Triggering of the *Ms* 6.9 1980 Irpinia Earthquake

Similar to seismicity triggered by wastewater injection (van der Elst et al., 2016), intense groundwater recharge of karst aquifers may temporarily increase the probability of earthquake occurrence at a wide range of magnitudes. Reliable catalogs are not available to detect a significant increment of seismicity before the 23 November 1980, M_S 6.9, earthquake. Analyses of century-long rainfall and spring discharge time series (Figure 5a), however, show that exceptional recharge conditions preceded the 1980 event and may have temporarily increased the probability for an earthquake to occur. The cumulative distribution of the 1920–2018 discharge values shows that the raw value observed on 23 November 1980 had been exceeded by 28.0% of the observations, whereas its low-pass filtered value, more indicative of multiannual state of recharge, had only been exceeded by 1.1% of the observations (Figure 5b). Rainfall cumulated over the previous 5 years recorded at the Serino rain gauges (located 27 km from Caposele spring; Figure 1) confirm the hypothesis of multiannual recharge showing a continuous increase starting in 1975 (gray area in Figure 5a). At the height of the high multiannual groundwater recharge, exceptional rainfall occurred from 9 to 13 October 1980 releasing ~ 30% (500 mm) of the average cumulative precipitation (Figure 5b) and continuing in the following month to reach ~ 55% of the average yearly amount on the eve of the earthquake. During this exceptional rainfall event the discharge of the Caposele spring was continuously decreasing (Figure 5c) implying that all

the infiltrated recharge was stored in the conduits network. The spring significantly increased its discharge (Muir-Wood & King, 1993) only after the 23 November 1980 Irpinia, M_S 6.9, earthquake reaching its maximum historical value on 19 January 1981 (Fiorillo, 2009; 7.32 m^3/s). The large, exceptional rainfall preceding the earthquake may have flooded the karst conduits by concentrated recharge resulting in an additional increment of the hydraulic head proportional to the height of the interconnected water column above the water table. Considering the ~700-m elevation difference between the reconstructed water table and the maximum recharge area (supporting information Figure S6), a hydraulic head variation of several megapascals may had additionally loaded upon the fluid-saturated, poroelastic crust. The hydrological conditions at the eve of the 1980 earthquake thus appears to result from the rare combination of high multiannual recharge and exceptional rainfall concentrated in a few days.

The analysis of seismic moment budget constrained by geodetic data and historical seismicity (D'Agostino, 2014) requires a $M \geq 6.5$ event to strike, on average, every 240–600 years in any ~ 50 km-long section of the Central-Southern Apennines. Considering the elapsed time since the previous $M \geq 6.5$ event in the Irpinia region (1694, Rovida et al., 2016; Galli & Peronace, 2014), a sufficient level of tectonic strain may have loaded the IFZ to require only a minor contribution from hydrological forcing to finally strike in 1980. In view of the high strain sensitivity of the IFZ to groundwater recharge we suggest that favorable hydrological stresses may have triggered the 1980 earthquake.

7. Conclusions

Our results document the high sensitivity of crustal strain to hydrological forcing by karst aquifers in the Southern Apennines. It is likely that our simple modeling approach to poroleastic deformation neglects two important aspects: the first is related to significant depth variations of the AP whose top boundary lies at 3.5–4 km near the southeastern part of the IFZ but varies substantially beneath the karst aquifers elsewhere in the Southern Apennines (Nicolai & Gambini, 2007). The second aspect is related to the hydrologically related volumetric deformation within the AP. This volumetric deformation may be associated with diffusion of pore pressure variations and migration of seismicity possibly contributing to the 0.1–0.2 years time lag between the surface hydrological forcing and the deeper seismicity.

One important finding of this study underlines the role of shallow poroelastic strain of karst aquifers in modulation of deeper seismicity and the importance of geodetic data for robust hydromechanical characterization of the upper crust. More generally, the assumption of a hydraulically connected fracture system between the surface and hypocentral depths may lead to incorrect inferences about the hydromechanical structure of the crust based only on spatiotemporal patterns of seismicity.

The retrospective analysis of hydrological conditions at the time of the 1980 Irpinia, M_S 6.9, earthquake using century-long hydrological time series shows that a combination of high multiannual recharge and intense seasonal rainfall induced favorable stress conditions for nucleation and propagation of a large event. Although assessing the general significance of hydrological triggering requires a thorough statistical evaluation, our observations support the hypothesis that large earthquakes might also be triggerable from low-amplitude hydrological stress modulation (Johnson et al., 2017). If the mechanism that we describe is characteristic of tectonically active karst regions, earthquake occurrence in large parts of the Mediterranean-Alpine belt can be influenced by groundwater recharge.

Acknowledgments
We thank all the personnel involved in the maintenance of the seismic, geodetic, and hydrological monitoring networks; James D. P. Moore for insightful advices on strain modeling; and Adrian Borsa for discussions on hydrological forcing. We thank the Editor Lucy Flesch and the Reviewers Bill Hammond and Kristel Chanard for careful and constructive reviews. Figures were produced with the GMT software package (Wessel et al., 2013).

References

Ader, T., Lapusta, N., Avouac, J., & Ampuero, J. (2014). Response of rate-and-state seismogenic faults to harmonic shear-stress perturbations. *Geophysical Journal International*, *198*, 385–413. https://doi.org/10.1093/gji/ggu144

Aki, K. (1965). Maximum likelihood estimate of b in the formula log n = a - bm and its confidence limits. *Bulletin of the Earthquake Research Institute*, *43*, 237–239.

Allocca, V., Manna, F., & De Vita, P. (2014). Estimating annual groundwater recharge coefficient for karst aquifers of the southern Apennines (Italy). *Hydrology and Earth System Sciences*, *18*(2), 803–817. https://doi.org/10.5194/hess-18-803-2014

Amoroso, O., Ascione, A., Mazzoli, S., Virieux, J., & Zollo, A. (2014). Seismic imaging of a fluid storage in the actively extending Apennine mountain belt, southern Italy. *Geophysical Research Letters*, *41*, 3802–3809. https://doi.org/10.1002/2014GL060070

Amoroso, O., Russo, G., De Landro, G., Zollo, A., Garambois, S., Mazzoli, S., et al. (2017). From velocity and attenuation tomography to rock physical modeling: Inferences on fluid-driven earthquake processes at the Irpinia fault system in southern Italy. *Geophysical Research Letters*, *44*, 6752–6760. https://doi.org/10.1002/2016GL072346

Avallone, A., Selvaggi, G., D'Anastasio, E., D'Agostino, N., Pietrantonio, P., Riguzzi, F., & Zarrilli, L. (2010). The ring network: Improvement of a GPS velocity field in the central Mediterranean. *Annals of Geophysics*, *53*(2), 39–54.

Barbot, S., Moore, J., & Lambert, V. (2017). Displacement and stress associated with distributed anelastic deformation in a half-space. *Bulletin of the Seismological Society of America*, *107*(2), 821. https://doi.org/10.1785/0120160237

Bernard, P., & Zollo, A. (1989). The Irpinia (Italy) 1980 earthquake: Detailed analysis of a complex normal faulting. *Journal of Geophysical Research*, *94*(B2), 1631–1647. https://doi.org/10.1029/JB094iB02p01631

Bertiger, W., Desai, S., Haines, B., Harvey, N., Moore, A., Owen, S., & Weiss, J. (2010). Single receiver phase ambiguity resolution with GPS data. *Journal of Geodesy*, *84*(5), 327–337. https://doi.org/10.1007/s00190-010-0371-9

Bettinelli, P., Avouac, J., Flouzat, M., Bollinger, L., Ramillien, G., Rajaure, S., & Sapkota, S. (2008). Seasonal variations of seismicity and geodetic strain in the Himalaya induced by surface hydrology. *Earth and Planetary Science Letters*, *266*(3), 332–344. https://doi.org/10.1016/j.epsl.2007.11.021

Blewitt, G., Kreemer, C., Hammond, W., & Gazeaux, J. (2016). Midas robust trend estimator for accurate GPS station velocities without step detection. *Journal of Geophysical Research: Solid Earth*, *121*, 2054–2068. https://doi.org/10.1002/2015JB012552

Christiansen, L., Hurwitz, S., & Ingebritsen, S. (2007). Annual modulation of seismicity along the San Andreas Fault near Parkfield, CA. *Geophysical Research Letters*, *34*, L04306. https://doi.org/10.1029/2006GL028634

Craig, T., Chanard, K., & Calais, E. (2017). Hydrologically-driven crustal stresses and seismicity in the new Madrid seismic zone. *Nature Communications*, *8*(1), 2143. https://doi.org/10.1038/s41467-017-01696-w

D'Agostino, N. (2014). Complete seismic release of tectonic strain and earthquake recurrence in the Apennines (Italy). *Geophysical Research Letters*, *41*, 1155–1162. https://doi.org/10.1002/2014GL059230

De Matteis, R., Matrullo, E., Rivera, L., Stabile, T. A., Pasquale, G., & Zollo, A. (2012). Fault delineation and regional stress direction from the analysis of background microseismicity in the southern Apennines, Italy, short notes. *Bulletin of the Seismological Society of America*, *102*(4), 1899. https://doi.org/10.1785/0120110225

Fiorillo, F. (2009). Spring hydrographs as indicators of droughts in a karst environment. *Journal of Hydrology*, *373*(3), 290–301. https://doi.org/10.1016/j.jhydrol.2009.04.034

Fiorillo, F., Petitta, M., Preziosi, E., Rusi, S., Esposito, L., & Tallini, M. (2015). Long-term trend and fluctuations of karst spring discharge in a Mediterranean area (central-southern Italy). *Environmental Earth Sciences*, *74*(1), 153–172. https://doi.org/10.1007/s12665-014-3946-6

Galli, P., & Peronace, E. (2014). New paleoseismic data from the Irpinia fault. A different seismogenic perspective for southern Apennines (Italy). *Earth-Science Reviews*, *136*, 175–201. https://doi.org/10.1016/j.earscirev.2014.05.013

Ghil, M., Allen, M., Dettinger, M., Ide, K., Kondrashov, D., Mann, M. E., et al. (2002). Advance spectral methods for climatic time series. *Reviews of Geophysics*, *40*(1), 1003. https://doi.org/10.1029/2000RG000092

Hainzl, S., Kraft, T., Wassermann, J., Igel, H., & Schmedes, E. (2006). Evidence for rainfall-triggered earthquake activity. *Geophysical Research Letters*, *33*, L19303. https://doi.org/10.1029/2006GL027642

Heki, K. (2003). Snow load and seasonal variation of earthquake occurrence in Japan. *Earth and Planetary Science Letters*, *207*(1), 159–164. https://doi.org/10.1016/S0012-821X(02)01148-2

Improta, L., De Gori, P., & Chiarabba, C. (2014). New insights into crustal structure, Cenozoic magmatism, CO_2 degassing, and seismogenesis in the southern Apennines and Irpinia region from local earthquake tomography. *Journal of Geophysical Research: Solid Earth*, *119*, 8283–8311. https://doi.org/10.1002/2013JB010890

Johnson, C., Fu, Y., & Bürgmann, R. (2017). Seasonal water storage, stress modulation, and California seismicity. *Science*, *356*(6343), 1161–1164. https://doi.org/10.1126/science.aak9547

Lomax, A., Michelini, A., & Curtis, A. (2009). Earthquake location, direct, global-search methods. In R. A. Meyers (Ed.), *Encyclopedia of Complexity and System Science*, Part 5 (pp. 2449–2473). New York: Springer. https://doi.org/10.1007/978-0-387-30440-3

Lomax, A., Virieux, J., Volant, P., & Berge, C. (2000). Probabilistic earthquake location in 3D and layered models: Introduction of a Metropolis-Gibbs method and comparison with linear locations. In C. H. Thurber & N. Rabinowitz (Eds.) *Advances in seismic event location* (pp. 101–134). Amsterdam: Kluwer.

Métois, M., D'Agostino, N., Avallone, A., Chamot-Rooke, N., Rabaute, A., Duni, L., et al. (2015). Insights on continental collisional processes from GPS data: Dynamics of the peri-adriatic belts. *Journal of Geophysical Research: Solid Earth*, *120*, 8701–8719. https://doi.org/10.1002/2015JB012023

Miller, S. A. (2008). Note on rain-triggered earthquakes and their dependence on karst geology. *Geophysical Journal International*, *173*(1), 334–338. https://doi.org/10.1111/j.1365-246X.2008.03735.x

Muir-Wood, R., & King, G. (1993). Hydrological signatures of earthquake strain. *Journal of Geophysical Research*, *98*(B12), 22,035–22,068. https://doi.org/10.1029/93JB02219

Nicolai, C., & Gambini, R. (2007). Structural architecture of the Adria platform-and-basin system. *Italian Journal of Geosciences*, *7*, 21–37.

Reasenberg, P. (1985). Second-order moment of central california seismicity, 1969-1982. *Journal of Geophysical Research*, *90*(B7), 5479–5495. https://doi.org/10.1029/JB090iB07p05479

Rebischung, P., Griffiths, J., Ray, J., Schmid, R., Collilieux, X., & Garayt, B. (2012). IGS08: The IGS realization of ITRF 2008. *GPS Solutions*, *16*(4), 483–494. https://doi.org/10.1007/s10291-011-0248-2

Roeloffs, E. (1988). Fault stability changes induced beneath a reservoir with cyclic variations in water level. *Journal of Geophysical Research*, *93*(B3), 2107–2124. https://doi.org/10.1029/JB093iB03p02107

Rovida, A., Locati, M., Camassi, R., Lolli, B., & Gasperini, P. (2016). CPTI15, the 2015 version of the parametric catalogue of Italian earthquakes (Tech. Rep.): Istituto Nazionale di Geofisica e Vulcanologia, https://emidius.mi.ingv.it/CPTI15-DBMI15. https://doi.org/10.6092/INGV.IT-CPTI15

Saar, M., & Manga, M. (2003). Seismicity induced by seasonal groundwater recharge at Mt. Hood, Oregon. *Earth and Planetary Science Letters*, *214*(3), 605–618. https://doi.org/10.1016/S0012-821X(03)00418-7

Schorlemmer, D., & Gerstenberger, M. C. (2007). Relm testing center. *Seismological Research Letters*, *78*(1), 30. https://doi.org/10.1785/gssrl.78.1.30

Segall, P. (1989). Earthquakes triggered by fluid extraction. *Geology*, *17*(10), 942. https://doi.org/10.1130/0091-7613(1989)017<0942:ETBFE>2.3.CO;2

Shi, Y., & Bolt, B. (1982). The standard error of the magnitude-frequency b value. *Bulletin of the Seismological Society of America*, *72*(5), 1677.

Silverii, F., D'Agostino, N., Borsa, A. A., Calcaterra, F., Gambino, P., Giuliani, R., & Mattone, M. (2019). Transient crustal deformation from karst aquifers hydrology in the Apennines (Italy). *Earth and Planetary Science Letters*, *506*, 23–37. https://doi.org/10.1016/j.epsl.2018.10.019

Silverii, F., D'Agostino, N., Métois, M., Fiorillo, F., & Ventafridda, G. (2016). Transient deformation of karst aquifers due to seasonal and multi-year groundwater variations observed by GPS in southern Apennines (Italy). *Journal of Geophysical Research: Solid Earth*, *121*, 8315–8337. https://doi.org/10.1002/2016JB013361

Talwani, P., Chen, L., & Gahalaut, K. (2007). Seismogenic permeability, k_s. *Journal of Geophysical Research*, *112*, B07309. https://doi.org/10.1029/2006JB004665

van Dam, T., Wahr, J., Milly, P., Shmakin, A., Blewitt, G., Lavallée, D., & Larson, K. M. (2001). Crustal displacements due to continental water loading. *Geophysical Research Letters*, *28*(4), 651–654. https://doi.org/10.1029/2000GL012120

van der Elst, N. J., Page, M., Weiser, D. A., Goebel, T., & Hosseini, S. M. (2016). Induced earthquake magnitudes are as large as (statistically) expected. *Journal of Geophysical Research: Solid Earth*, *121*, 4575–4590. https://doi.org/10.1002/2016JB012818

Wessel, P., Smith, W. H. F., Scharroo, R., Luis, J., & Wobbe, F. (2013). Generic Mapping Tools: Improved version released. *Eos, Transactions American Geophysical Union*, *94*(45), 409–410. https://doi.org/10.1002/2013EO450001

Wiemer, S. (2001). A software package to analyze seismicity: ZMAP. *Seismological Research Letters*, *72*(3), 373. https://doi.org/10.1785/gssrl.72.3.373

Woessner, J., & Wiemer, S. (2005). Assessing the quality of earthquake catalogues: Estimating the magnitude of completeness and its uncertainty. *Bulletin of the Seismological Society of America*, *95*(2), 684. https://doi.org/10.1785/0120040007